A Low-Cost Structure for Reducing Reflection Loss in Intelligent Reflecting Surface of Liquid Crystal

Yue Cui, *Graduate Student Member, IEEE*, Hiroyasu Sato, *Member, IEEE*, Yosei Shibata, Takahiro Ishinabe, *Member, IEEE*, Hideo Fujikake, *Senior Member, IEEE*, and Qiang Chen, *Senior Member, IEEE*

***Abstract*—In this letter, a structure to reduce the reflection loss in intelligent reflecting surface of liquid crystal (IRS-LC) is proposed. The loss in IRS-LC is analyzed, indicating that the electric field in the liquid crystal (LC) is a primary cause. To address this issue, a structure by introducing a loss suppression structure (LSS) beneath the LC layer is presented.Theoretical analysis confirms the low reflection loss characteristic of the structure, and a 15×15 prototype IRS-LC array is fabricated and measured. Simulated and measurement results show that the proposed IRS-LC has a maximum reflection loss reduction of 11.3dB, a magnitude variation reduction of 8.5 dB at 40.3 GHz, and a reflection phase range of 204 degrees. The results validates the proposed structure in reducing the reflection loss. Furthermore, the proposed IRS-LC structure has the advantages of low cost and easy processing.**

***Index Terms*—Liquid crystal (LC), intelligent reflecting surface (IRS), reflection loss, low cost, multilayer.**

I. Introduction

REFLECTARRAY (RA) is an effective means to increase the electromagnetic (EM) signal level in the target area without excessive power consumption, and its two-dimensional arrangement makes it easy to integrate into structures such as building facades and interior walls [1]–[4]. However, traditional RA that focuses scattered EM waves into a single direction is inadequate for the complex coverage requirements. As a result, the intelligent reflecting surface (IRS) which can change beam direction has gained widespread attention [5]. Numerous studies on IRS have been conducted so far [6]–[14], including such as the use of diodes [6]–[8], mechanical methods [9], [10] and nematic liquid crystal (LC) [10]–[15]. The rod-shaped molecular structure of nematic LC can be deflected continuously by an external electric or magnetic field, resulting in a corresponding continuous change in its permittivity. This feature of LC allows IRS to continuously shift the beam direction, which is the primary advantage of intelligent reflecting surfaces of liquid crystal (IRS-LC).In addition, the ease of applying an external electric field to the LC through bias lines further contributes to the design simplicity and cost-effectiveness of the IRS-LC.

This work was supported by the Ministry of Internal Affairs and Communications in Japan (JPJ000254).(*Corresponding Author: Yue Cui*)

Yue Cui, Hiroyasu Sato and Qiang Chen are with the Department of Communications Engineering, Tohoku University, Sendai 980-8579, Japan. (e-mail: cui.yue.t4@dc.tohoku.ac.jp)

Yosei Shibata, Takahiro Ishinabe and Hideo Fujikake are with the Department of Electronic Engineering, Tohoku University, Sendai 980-8579, Japan.

However, IRS-LC has a disadvantage of high reflection loss. Reflection loss not only results in dissipation of the incident EM wave but also introduces significant variations in reflection magnitude at different reflection phases, leading to a decrease in the aperture efficiency of IRS-LC [16]. There have been few studies on reducing the reflection loss of IRS-LC [17], [18]. One approach to reduce the reflection loss by increasing the thickness of the LC layer [17]. However, a thick LC requires a large bias voltage to control the LC and long response time, thereby increasing the cost [19]. Another work introduced multi-resonant structure to reduce the reflection loss [18]. However, the cost was high due to its metal via-hole structure in the superstrate.

To address this issue, a novel structure by introducing a loss suppression structure (LSS) beneath the LC layer is proposed in this letter. The LSS consists of a substrate and an air layer. Theoretical analysis shows a strong correlation between the electric field in the LC and the reflection loss.The effective permittivity of the LSS can influence the electric field in the LC, and can be controlled by adjusting the thickness of the air layer. As a result, the thickness of the air layer affects the reflection loss and magnitude variation of the IRS-LC. Additionally, 3D printed fixture is used to control the thickness of the air layer in a cost-effective manner. The proposed IRS-LC structure has reduced reflection loss, low cost, and easy processing characteristics.

II. Design and Theoretical Analysis

A. Proposed structure

The proposed IRS-LC unit cell structure is shown in Fig. 1. It consists of four parts arranged from top to bottom as shown in Fig. 1(a): the superstrate, the LC layer, the LSS, and the metal ground. The LSS is composed of a substrate and an air layer. Two identical metal patches are positioned on the upper and lower surfaces of the LC layer, with each patch connected to a bias line to apply bias voltage, as shown in Fig.1 (b) and (c). Fig.1 (d) and (e) illustrate the schematic of the LC molecules under different bias voltages. When no bias voltage is applied, the director of the LC molecules aligns in the y-direction due to the presence of polymide films with y-direction microgrooves that are coated on the patches. The corresponding relative permittivity ($\varepsilon_{r\perp}$) of the LC is 2.5, and the loss tangent ($\tan\delta_{\perp}$) is 0.02. Conversely, when the full bias voltage is applied, the director of the LC molecules deflects to the direction of the applied electric field. In this

case, the corresponding relative permittivity ($\varepsilon_{r//}$) and loss tangent ($\tan\delta_{//}$) are 3 and 0.007, respectively. Additionally, to ensure smooth surfaces for the polymide film coating process, glass ($\varepsilon_r = 3.7, \tan\delta = 0.007$) is chosen as the material for both the superstrate and substrate.

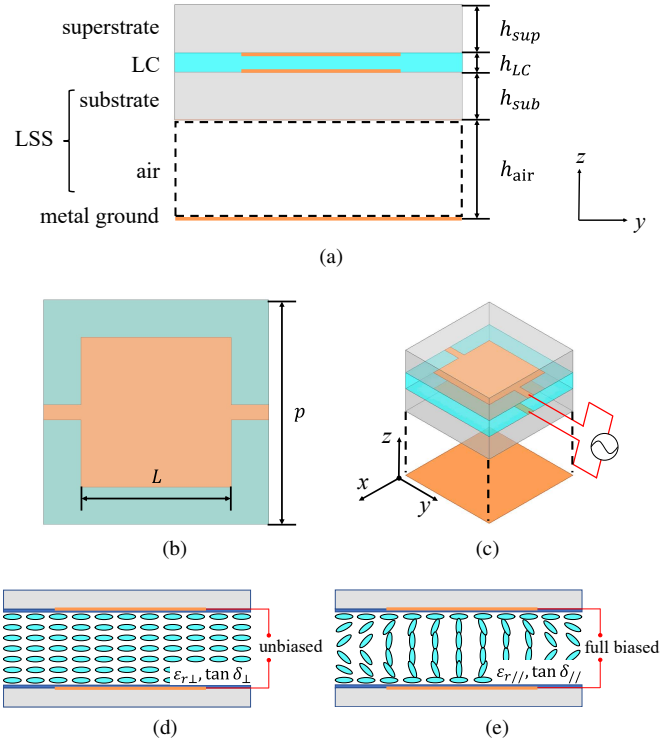

Fig. 1. The (a) side view, (b) top view and (c) bird eye view of the proposed IRS-LC unit cell structure, and schematics of the LC molecules under (d) unbiased voltage and (e) full biased voltage. p=3 mm, L=2 mm, h_{sup}=0.7 mm, h_{LC}=0.1 mm, h_{sub}=0.7 mm.

B. Theoretical Analysis

When electromagnetic waves propagate through a dielectric medium, a portion of the energy is dissipated due to the conductivity (σ) of the dielectric material [20]:

$$P_{loss} = \frac{\sigma}{2}\iiint_v |\boldsymbol{E}|^2 dv \tag{1}$$

where P_{loss} represents the time-average dissipated power. In the case of IRS-LC, the dissipation of incident energy in LC, as well as other substrates and metals, is referred to as reflection loss. Due to the high loss tangent ($\tan\delta = \sigma/\omega\varepsilon$) exhibited by LC, the IRS-LC reflection loss is primarily attributed to the energy dissipated in LC. According to equation (1), there are two approaches to reducing the reflection loss: decreasing the conductivity of the LC and minimizing the electric field in the LC. For a given LC, reducing the electric field inside the LC layer is the key factor in suppressing reflection loss.Conventional IRS-LC consists of three layers: a superstrate containing metal resonance structure, a LC layer, and a metal ground. To minimize costs, the thickness of the LC layer in IRS-LC is commonly designed in micron range. However, the thickness of LC layer is too thin compared to the wavelength, resulting in a significant electric field within the layer during resonance and lead to a high reflection loss. Increasing the thickness of the LC layer is a effective approach to reduce the electric field in the LC layer, but it will increase the cost and response time. To address this issue, the proposed IRS-LC unit cell incorporates a LSS beneath the LC layer. The LSS enables a reduction in the electric field while maintaining a thin LC layer, without incurring additional costs.

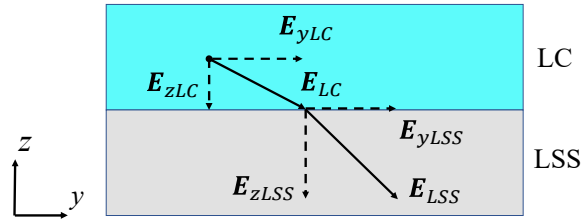

Fig. 2. The schematic of electric field at the interface between the LC layer and the LSS.

When a plane EM wave illuminates the proposed IRS-LC, the metal patch generates induced current. Subsequently, the induced current excites an electric field containing components in propagation direction ($\boldsymbol{E}_z$), which are not present in the incident plane wave [21]. The schematic of electric field at the interface between the LC layer and the LSS is shown in Fig.2. For simplicity, $\boldsymbol{E}_y$ is adopted to represent the parallel component. According to the Maxwell-Faraday equation and the Gauss's law [22], the parallel and perpendicular components at the interface can be written as:

$$|\boldsymbol{E}_{yLC}| = |\boldsymbol{E}_{yLSS}| \tag{2}$$

$$\frac{\varepsilon_{LSS}}{\varepsilon_{LC}} = \frac{|\boldsymbol{E}_{zLC}|}{|\boldsymbol{E}_{zLSS}|} \tag{3}$$

where ε_{LC} and ε_{LSS} represent the permittivity of the LC and the effective permittivity of the LSS.According to Equation (2) and (3), it is evident that $|\boldsymbol{E}_{yLC}|$ is equal to $|\boldsymbol{E}_{yLSS}|$. Additionally, decreasing the ε_{LSS} results in a reduction in $|\boldsymbol{E}_{zLC}|/|\boldsymbol{E}_{zLSS}|$. Therefore, the overall electric field in the LC layer decreases as ε_{LSS} reduces. This reduction in ε_{LSS} can be achieved by adjusting the thickness of the air layer (h_{air}) [23]:

$$\varepsilon_{LSS} = \frac{(h_{sub} + h_{air})\varepsilon_{sub}\varepsilon_{air}}{h_{sub}\varepsilon_{air} + h_{air}\varepsilon_{sub}} \tag{4}$$

where ε_{sub} and ε_{air} represent the permittivity of the substrate and the air layer, respectively.Increasing the thickness of the air layer (h_{air}) causes the ε_{LSS} to decrease and converge to ε_0. Consequently, the electric field in the LC layer and the reflection loss of the proposed IRS-LC decrease with increasing h_{air}.

The aforementioned theoretical analysis was validated through full-wave simulation.The reflection magnitudes under different h_{air} are presented in Fig. 3 (a). It can be observed that the reflection magnitude increases with increasing h_{air}, indicating a reduction of the reflection loss. The presence of the LSS in the structure leads to a significant reduction in reflection loss, exhibiting reductions of 11.3 dB under no bias voltage and 6.8 dB under full bias voltage, in comparison to

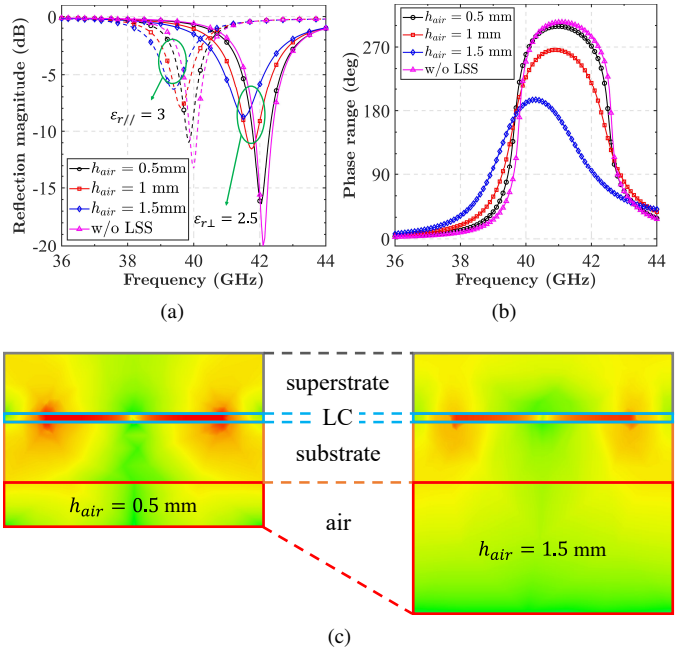

Fig. 3. The simulated (a) reflection magnitude, (b) the reflection phase range and (c) the electric field of the proposed IRS-LC unit cell.

the structure without the LSS. The larger reduction of reflection loss under full bias voltage compared to no bias voltage is attributed to the varying conductivity of the LC material under different bias voltages. The reflection phase range, defined as the phase difference between $\varepsilon_{r\perp}$ and $\varepsilon_{r//}$ of the LC, decreases with increasing h_{air}, as shown in Fig. 3 (b). This is due to the increased thickness of the air layer reduces the electric field within the LC layer, which in turn diminishes the ability of the LC to adjust the reflection phase. Fig. 3 (c) illustrates the simulated electric field for the various thicknesses of air layer. The electric field within LC layer decreases as the h_{air} increases from 0.5mm to 1.5mm, which is consistent with the theoretical analysis. The reduction in electric field within the LC layer leads to reduced reflection loss. However, it also results in a diminished capacity to control the reflection phase of the proposed IRS-LC. Therefore, it is a trade-off between reflection loss and reflection phase that must be considered when selecting the thickness of the air layer.

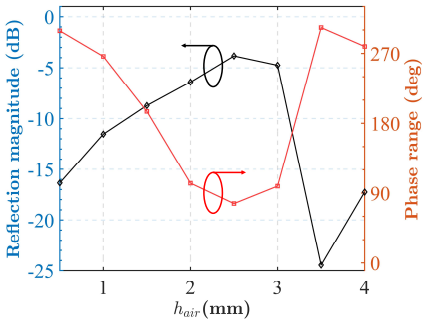

Fig. 4. The minimum reflection magnitude and phase range under different h_{air}.

In order to select a appropriate air layer thickness, the minimum reflection magnitude as well as the phase range were simulated for various h_{air} at single frequency, as shown in Fig. 4. It can be seen that the reflection magnitude exhibits periodic behavior within a range of approximately half-wavelength. This is due to varying the h_{air} changes the position of the LC layer on the standing wave formed by the metal ground, which lead to periodic variations in the electric field within the LC layer. Additionally, the phase range decreases as the reflection magnitude increases. Therefore, a suitable value for h_{air} needs to be selected to achieve both low reflection loss and acceptable phase range. In this study, the phase range was set to be at least 180 degrees to ensure the capability of the beam scanning of the proposed IRS-LC [24]–[26]. And the corresponding h_{air} is determined to be 1.5 mm.

III. Measurement

A 15×15 prototype IRS-LC array was fabricated, comprising three main components: the superstructure, the metal ground, and 3D printed fixtures, as depicted in Fig. 5 (a). The superstructure is composed of the superstrate, the LC layer, and the substrate. Fig. 5 (b) shows the side view of the assembled IRS-LC array. The air layer is formed by the 3D printed fixtures, and the thickness can be adjusted by using different fixtures. The reflection loss and phase range of the prototype IRS-LC array were measured using a lens-loaded printed antipodal fermi tapered slot antenna (APFA) [27] with Keysight boldsymboltor Network Analyzer P5008A. The permittivity of the LC was adjusted by applying a low-frequency voltage of 1 kHz to the electrodes (i.e., patches). Since the distance between the electrodes is fixed, the proposed structure preserves the capacity to control the permittivity of the LC.

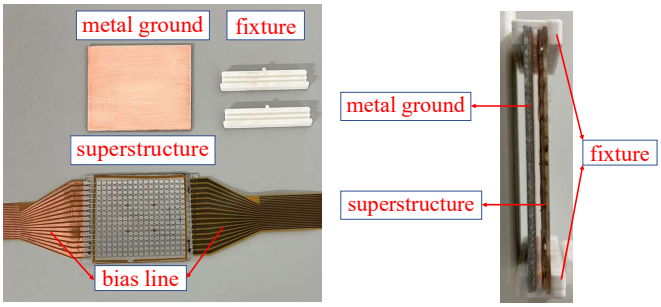

Fig. 5. (a) Unassembled and (b) side view of the assembled prototype IRS-LC array.

Since the simulated results in the previous section were analyzed under the assumption of plane EM wave incidence, it is desirable to measure the prototype under the same conditions. The lens-loaded APFA is used to generate quasi-plane EM wave, as shown in Fig.6 (a). The magnitude and phase distribution at a distance of 1.3 m from the lens-loaded APFA were measured in X plane and Y plane, as shown in Fig. 6 (b) and (c). In the band of 39-42 GHz, the maximum magnitude variation is 0.8 dB and the maximum phase variation is 8 degrees. As the phase variation is less than 22.5 degrees,

which can be derived from the far-field condition [16], the lens-loaded APFA is capable of providing a quasi-plane EM wave in the frequency range of 39 GHz to 42 GHz within a 50 mm×50 mm area.

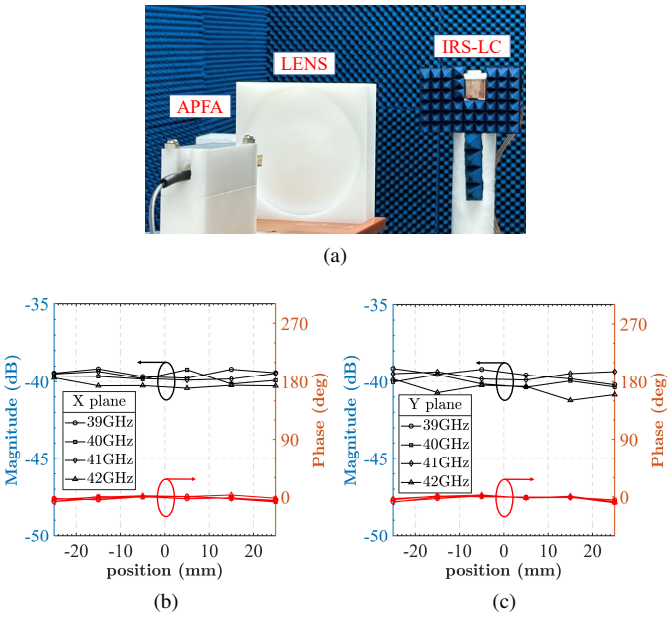

Fig. 6. (a) Measurement environment, (b) magnitude and phase distribution of the lens-loaded APFA in the X plane and (c) Y plane.

Fig. 7 presents the measurement results for various air layer thicknesses. As shown in Fig. 7 (a), increasing the h_{air} leads to a reduction in reflection loss. Compared to $h_{air} = 0.5$ mm, there is an 8.8 dB reduction in reflection loss when no bias voltage is applied ($\varepsilon_{r\perp}$), and a 3 dB reduction at full bias voltage ($\varepsilon_{r//}$). Fig. 7 (b) shows that the reflection phase range decreases from 290 degrees to 204 degrees as the h_{air} increases from 0.5 mm to 1.5 mm.

The reflection magnitude and phase versus bias voltage were also measured to evaluate the proposed IRS-LC structure, as shown in Fig. 7 (c) and (d). The frequency was fixed at 40.3 GHz, and the air layer thicknesses were chosen as 0.5 mm, 1 mm, and 1.5 mm, respectively. The reflection magnitude variation reduced from 11.9 dB at $h_{air} = 0.5$ mm to 3.4 dB at $h_{air} = 1.5$ mm. Meanwhile, the phase variation reduced from 275 degrees at $h_{air} = 0.5$ mm to 204 degrees at $h_{air} = 1.5$ mm. Table I shows the performance comparison of the IRS-LC. In comparison to previous works, the proposed IRS-LC features a thin LC layer, making it cost-effective. Despite the introduction of the LSS increasing the total thickness, it remains within a reasonable range for IRS applications [28]–[30]. Additionally, the proposed design achieves a significant reduction in reflection loss and low reflection magnitude variation, which can be primarily attributed to the LSS. The measured results validating the effectiveness of the proposed structure for reducing the reflection loss of IRS-LC while maintaining an acceptable reflection phase range, low cost, and easy processing characteristics.

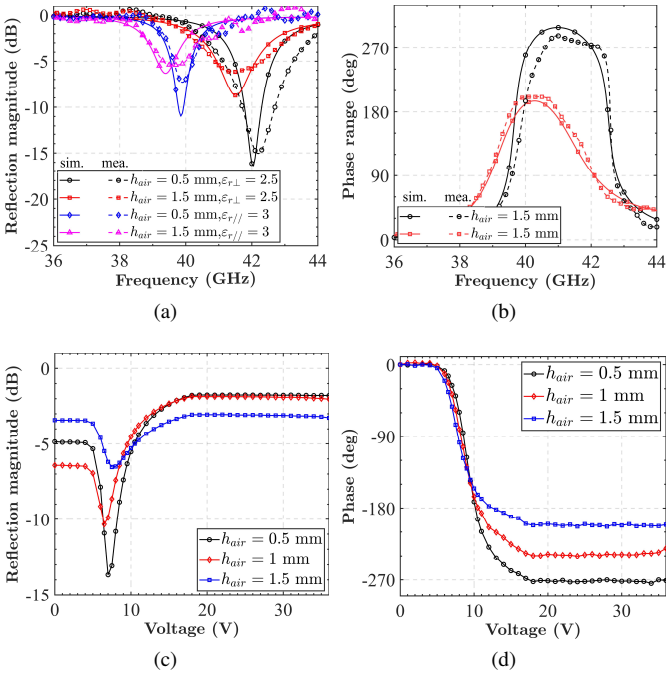

Fig. 7. Measured (a) reflection magnitude and (b) reflection phase range versus frequency, (c) reflection magnitude and (d) reflection phase versus bias voltage at 40.3 GHz.

TABLE I
COMPARISON WITH PRIOR WORKS

Feature	[13]	[17]	[18]	[31]	This work
Frequency (GHz)	10	10	10	104	40.3
LC thickness(μm)	500	500	250	80	100
Total thickness(λ)	0.021	0.018	0.039	0.218	0.403
Max. RL reduction(dB)	-	2	6	-	11.3
Reflection magnitude variation(dB)	32	-	2	11.7	3.4

RL: reflection loss.

IV. CONCLUSION

This letter proposed a novel structure to reduce the reflection loss of IRS-LC by introducing a LSS beneath the LC layer. Theoretical analysis reveals that the effective permittivity of the LSS is related to the electric field in the LC layer, which in turn affects the reflection loss of the IRS-LC. By adjusting the thickness of the air layer in the LSS, the effective permittivity can be controlled, thereby reducing the reflection loss of the IRS-LC. A 15×15 prototype array of the proposed IRS-LC structure is fabricated, experiment results indicated that the structure effectively reduces the reflection loss and magnitude variation of the IRS-LC, while maintaining a acceptable reflection phase range. Furthermore, the proposed IRS-LC structure has advantages of cost-effective and easy processing due to its simple structure, thin LC layer and 3D printed fixture, which making the structure a promising candidate for practical applications.

REFERENCES

[1] D. Berry, R. Malech, and W. Kennedy, "The reflectarray antenna," *IEEE Trans. Antennas Propag.*, vol. 11, no. 6, pp. 645–651, 1963.

[2] D. Pozar, S. Targonski, and H. Syrigos, "Design of millimeter wave microstrip reflectarrays," *IEEE Trans. Antennas Propag.*, vol. 45, no. 2, pp. 287–296, 1997.

[3] J. Huang and R. Pogorzelski, "A ka-band microstrip reflectarray with elements having variable rotation angles," *IEEE Trans. Antennas Propag.*, vol. 46, no. 5, pp. 650–656, 1998.

[4] J. Encinar, "Design of two-layer printed reflectarrays using patches of variable size," *IEEE Trans. Antennas Propag.*, vol. 49, no. 10, pp. 1403–1410, 2001.

[5] Q. Wu and R. Zhang, "Intelligent reflecting surface enhanced wireless network via joint active and passive beamforming," *IEEE Trans. Wireless Commun.*, vol. 18, no. 11, pp. 5394–5409, 2019.

[6] W. Wu, K.-D. Xu, Q. Chen, T. Tanaka, M. Kozai, and H. Minami, "A wideband reflectarray based on single-layer magneto-electric dipole elements with 1-bit switching mode," *IEEE Trans. Antennas Propag.*, vol. 70, no. 12, pp. 12 346–12 351, 2022.

[7] J. Han, L. Li, G. Liu, Z. Wu, and Y. Shi, "A wideband 1 bit 12 × 12 reconfigurable beam-scanning reflectarray: Design, fabrication, and measurement," *IEEE Antennas Wireless Propag. Lett.*, vol. 18, no. 6, pp. 1268–1272, 2019.

[8] S. V. Hum, M. Okoniewski, and R. J. Davies, "Modeling and design of electronically tunable reflectarrays," *IEEE Trans. Antennas Propag.*, vol. 55, no. 8, pp. 2200–2210, 2007.

[9] W. Menzel, D. Pilz, and M. Al-Tikriti, "Millimeter-wave folded reflector antennas with high gain, low loss, and low profile," *IEEE Antennas Propag. Mag.*, vol. 44, no. 3, pp. 24–29, 2002.

[10] X. Yang, S. Xu, F. Yang, M. Li, H. Fang, Y. Hou, S. Jiang, and L. Liu, "A mechanically reconfigurable reflectarray with slotted patches of tunable height," *IEEE Antennas Wireless Propag. Lett.*, vol. 17, no. 4, pp. 555–558, 2018.

[11] S. Bildik, S. Dieter, C. Fritzsch, W. Menzel, and R. Jakoby, "Reconfigurable folded reflectarray antenna based upon liquid crystal technology," *IEEE Trans. Antennas Propag.*, vol. 63, no. 1, pp. 122–132, 2015.

[12] X. Li, Y. Wan, J. Liu, D. Jiang, T. Bai, K. Zhu, J. Zhuang, and W.-Q. Wang, "Broadband electronically scanned reflectarray antenna with liquid crystals," *IEEE Antennas Wireless Propag. Lett.*, vol. 20, no. 3, pp. 396–400, 2021.

[13] M. Y. Ismail, R. Cahill, M. Amin, A. F. M. Zain, and M. K. Amin, "Phase range analysis of patch antenna reflectarray based on nematic liquid crystal substrate with dynamic rcs variation," in *2007 Asia-Pacific Microwave Conference*, 2007, pp. 1–4.

[14] W. Hu, R. Cahill, J. A. Encinar, R. Dickie, H. Gamble, V. Fusco, and N. Grant, "Design and measurement of reconfigurable millimeter wave reflectarray cells with nematic liquid crystal," *IEEE Trans. Antennas Propag.*, vol. 56, no. 10, pp. 3112–3117, 2008.

[15] X. Li, H. Sato, Y. Shibata, T. Ishinabe, H. Fujikake, and Q. Chen, "Development of beam steerable reflectarray with liquid crystal for both e-plane and h-plane," *IEEE Access*, vol. 10, pp. 26 177–26 185, 2022.

[16] P. Nayeri, F. Yang, and A. Z. Elsherbeni, *Reflectarray antennas: theory, designs, and applications*. John Wiley & Sons, 2018.

[17] M. Ismail and R. Cahill, "Application of liquid crystal technology for electronically scanned reflectarrays," in *2005 Asia-Pacific Conference on Applied Electromagnetics*, 2005, pp. 4 pp.–.

[18] H. Kim, J. Kim, and J. Oh, "Communication a novel systematic design of high-aperture-efficiency 2d beam-scanning liquid-crystal embedded reflectarray antenna for 6g fr3 and radar applications," *IEEE Trans. Antennas Propag.*, vol. 70, no. 11, pp. 11 194–11 198, 2022.

[19] P.-G. De Gennes and J. Prost, *The physics of liquid crystals*. Oxford university press, 1993, no. 83.

[20] W. L. Stutzman and G. A. Thiele, *Antenna theory and design*. John Wiley & Sons, 2012.

[21] C. A. Balanis, *Antenna theory: analysis and design*. John wiley & sons, 2016.

[22] D. Pozar, *Microwave Engineering, 4th Edition*. Wiley, 2011.

[23] M. F. Iskander, *Electromagnetic fields and waves*. Prentice Hall, 1992.

[24] H. Yang, F. Yang, S. Xu, Y. Mao, M. Li, X. Cao, and J. Gao, "A 1-bit 10 × 10 reconfigurable reflectarray antenna: Design, optimization, and experiment," *IEEE Trans. Antennas Propag.*, vol. 64, no. 6, pp. 2246–2254, 2016.

[25] P. Mei, S. Zhang, and G. F. Pedersen, "A low-cost, high-efficiency and full-metal reflectarray antenna with mechanically 2-d beam-steerable capabilities for 5g applications," *IEEE Trans. Antennas Propag.*, vol. 68, no. 10, pp. 6997–7006, 2020.

[26] W. Zhang, Y. Li, and Z. Zhang, "A reconfigurable reflectarray antenna with an 8 m-thick layer of liquid crystal," *IEEE Trans. Antennas Propag.*, vol. 70, no. 4, pp. 2770–2778, 2022.

[27] H. Sato, Y. Takagi, and K. Sawaya, "High gain antipodal fermi antenna with low cross polarization," *IEICE transactions on communications*, vol. 94, no. 8, pp. 2292–2297, 2011.

[28] M. R. Chaharmir and J. Shaker, "Design of a multilayer x-/ka-band frequency-selective surface-backed reflectarray for satellite applications," *IEEE Trans. Antennas Propag.*, vol. 63, no. 4, pp. 1255–1262, 2015.

[29] R. Deng, F. Yang, S. Xu, and M. Li, "An fss-backed 20/30-ghz dual-band circularly polarized reflectarray with suppressed mutual coupling and enhanced performance," *IEEE Trans. Antennas Propag.*, vol. 65, no. 2, pp. 926–931, 2017.

[30] L. Martinez-Lopez, R. Martinez-Lopez, J. Rodriguez-Cuevas, A. E. Martynyuk, and J. I. Martinez-Lopez, "A dual circularly-polarized multilayer reflective surface based on loaded ring slots," *IEEE Access*, vol. 9, pp. 6990–6999, 2021.

[31] G. Perez-Palomino, P. Baine, R. Dickie, M. Bain, J. A. Encinar, R. Cahill, M. Barba, and G. Toso, "Design and experimental validation of liquid crystal-based reconfigurable reflectarray elements with improved bandwidth in f-band," *IEEE Trans. Antennas Propag.*, vol. 61, no. 4, pp. 1704–1713, 2013.